Journal of Power Sources, 42 (1993) 71–88

Influence of antimony on the electrochemical behaviour and the structure of the lead dioxide active mass of lead/acid batteries

D. Pavlov, A. Dakhouche and T. Rogachev
Central Laboratory of Electrochemical Power Sources, Bulgarian Academy of Sciences, Sofia 1113 (Bulgaria)

Abstract

The effect of antimony on the formation of the skeleton structure of tubular electrodes filled with lead dioxide active mass (PAM) is investigated. Antimony is added as ions to the solution, as Sb_2O_3 or Sb_2O_5 to PAM, or as an additive to the electrode spine alloy. The effect of antimony on the crystallinity of PAM particles and agglomerates is examined. It is established that antimony increases the capacity of tubular powder electrodes when added either to the alloy or as antimony oxide to the PAM. It accelerates the processes of formation of the PAM skeleton structure and decreases the crystallinity of PAM particles and agglomerates. These effects of antimony are explained based on the concept of a gel-crystal structure for the PAM. Antimony improves the electron conductivity of gel zones. Its effect depends on the type and valency of the antimony ions, and on the density of the PAM.

Introduction

When Pb–Sb alloys used for the production of lead/acid battery positive grids were replaced with Pb-Ca alloys, it was found that the capacity of cycled lead dioxide plates declined rapidly to about 70–80% of the initial value. The positive plates were seemingly in good condition and a defined state-of-charge. It appeared that something had happened in the plates that was due to the lack of antimony in the grid alloy. Consequently, this phenomenon was called the 'antimony-free' effect. Later, Hollenkamp [1] referred to this effect as 'premature capacity loss' because of the early drop in capacity on cycling. Both terms are based on the result of the phenomenon rather than on its nature. A true understanding of the observed behaviour has yet to be reached.

The effect of antimony on the lead dioxide electrode system has long been the subject of scientific research [1–40]. Investigations have been carried out on the changes invoked by antimony on the properties and the structure of lead dioxide electrodes during anodic polarization or cathodic reduction in H_2SO_4 solution. The second research trend is directed towards studying the effect of antimony on the positive plates of lead/acid batteries, e.g., the changes in behaviour of the active mass or the corrosion layer covering the grid, or of both. These investigations have been based on the concept that both the anodic layer and the active mass are crystal systems composed mainly of α- and β-PbO_2, together with amorphous PbO_2. This strategy failed, however, to

0378-7753/93/$6.00

produce a satisfactory physical explanation of the effect of antimony on the electrochemical performance of battery plates.

A new approach to this problem has been suggested recently [41]. In this, the PAM is considered to be a gel-crystal system. The PAM agglomerates and particles are assumed to be built up of gel that is partially dehydrated to form α- or β-PbO_2 crystal zones. These crystal zones ('islands' in the gel) are electron conductive (n-type degenerate semiconductor). The gel zones are composed of hydrated polymer chains that exhibit both proton and electron conductivity. The electron conductivity is determined by the movement of electrons along the polymer chains. The latter play the role of electronic 'bridges' between the crystal zones ('island-bridge' electron conductivity). The aim of the present paper is to explain the effect of antimony on the electrochemical behaviour of the lead dioxide active mass in terms of this model for the PAM structure.

Experimental

Experimental methods

One of the major tasks of the present investigation is to establish the influence of antimony on the electrical behaviour of gel zones. The following indirect method was used: the active mass of positive battery plates (PAM) was removed from the grids of lead dioxide battery plates and dispersed into agglomerates and particles. The surfaces of the constituents consist of gel-like layers. The resulting powder was placed in tubular electrodes with lead spines. When such electrodes are immersed in H_2SO_4 solution and subjected to cycling, these particles and agglomerates are gradually interconnected to produce a skeleton. During the first several cycles, the capacity of the PAM is delivered only by those agglomerates that sustain electron transfer through their adjacent gel zones. Thus, the capacity of the powder electrode can be used as a measure of the electrical properties of the gel zones in the PAM. When antimony is added to the grid alloy or to the solution, the observed changes in capacity will be an indication of the influence of antimony on the electrical behaviour of gel zones.

PbO_2 powder preparation

Positive and negative plates were produced with pure-lead grids. The pastes were prepared from a 4.5% H_2SO_4/PbO mixture at 30–50 °C. Plate formation was carried out in H_2SO_4 solution of 1.05 sp.gr. Cells with 50% utilization of the positive active mass were assembled and subjected to five charge/discharge cycles at 100% depth-of-discharge (DOD). The active mass was removed from the grids, washed with water, dried at 60 °C for 1 h, and ground to powder. This powder was placed in a glass flask and then used to prepare tubular powder electrodes.

Tubular powder electrodes

The design of the tubular powder electrode has been reported previously [35]. The polyester-fabric tube was filled with PbO_2 powder of known weight. A threaded electrode spine was used with plugs at both ends that served to confine the powder within a definite volume of the tube. It was thus possible to control precisely the density of the powder in the tubular electrode. The diameters of the tube and spine were 9.0 mm and 4.0 mm, respectively. Electrodes with two powder densities (d) were predominantly used, namely, $d = 4.15$ g cm^{-3} (tube contained 11 g PAM), and $d =$ 3.80 g cm^{-3} (10 g PAM).

Cell design

Cells consisting of a tubular electrode, two negative plates with lead grids, and a $Hg/HgSO_4$ reference electrode, were assembled in glass containers. The electrolyte was 4.5 M H_2SO_4 (1.28 sp.gr.). The powder electrodes were subjected to the following preliminary treatment. The cells were left on open circuit for 30 min to allow the electrodes to soak up the solution. The electrodes were then charged at 15 mA cm^{-2} for 45 min to allow a corrosion layer to be formed on the surface of the spine. This was followed by a period of 10 min rest at open circuit, and a discharge at 15 mA cm^{-2} (i.e., $i = 10$ mA g^{-1} PAM at $d = 3.80$ g cm^{-3}, and $i = 9.1$ mA g^{-1} PAM at $d = 4.15$ g cm^{-3}) down to 0 mV.

About 15 cycles were conducted altogether, the electrode capacity was measured at each discharge. The tubular electrodes were then removed from the cells and the tubes were cut open without washing the electrodes from the H_2SO_4 solution. Samples were taken from the active mass and their crystallinity was determined through X-ray diffraction methods.

Other samples of the active mass were washed with water until neutral, then dried and subjected to scanning and transmission electron microscopy (SEM and TEM).

The samples were prepared for the SEM and TEM observations in the following way. Pieces of the dry active mass were placed in an ultrasonic alcohol bath and vibrated for 3 min to cause disintegration. The resultant suspension was filtered. Samples from the precipitate were taken with the help of a brush and spread over microscope copper nets covered with Formvar film. The nets were coated with a carbon layer and then placed in a JEOL 200 CX transmission electron microscope to examine the lead dioxide particles and agglomerates.

A scheme for investigating the effect of antimony

Antimony may be supposed to exert an influence on three zones of the electrode: (i) the active mass; (ii) the composition and properties of the corrosion layer; (iii) the contact of the corrosion layer with the active mass and the grid metal. In order to determine the effect of antimony on these three zones, antimony was added to:

- the 4.5 M H_2SO_4 solution, in concentrations 1×10^{-3}, 2×10^{-3} and 1×10^{-2} M Sb^{3+}
- the spine alloy, in concentrations 0.1, 0.2, 0.8, 2, 6 and 9 wt.% Sb
- the positive active mass as Sb_2O_3 or Sb_2O_5 (50 mg each)

The initial solution of antimony ions in 4.5 M H_2SO_4 was prepared by dissolving 1.5 g metal Sb in 200 ml concentrated H_2SO_4 with boiling. When cooled down, the solution was diluted with water to give 1.28 sp.gr. at 25 °C. The oversaturated solution was left to stand for 24 h and then filtered. The filtrate was left for a further 24 h and, if a residue still remained, the procedure was repeated until a stable saturated solution was obtained. A sample was taken from this solution and subjected to atomic absorption spectrophotometry (AAS) and inductively-coupled plasma spectroscopy (ICP) to determine the antimony content. An antimony concentration of 1.39 g dm^{-3} was established.

Results

Effect of active mass density

Tubular electrodes were prepared with various PbO_2 powder masses that yielded active mass densities between 3.40 and 4.15 g cm^{-3}. Figure 1 shows the curves of the specific capacity (A h g^{-1}) versus the number of cycles for electrodes with pure-lead

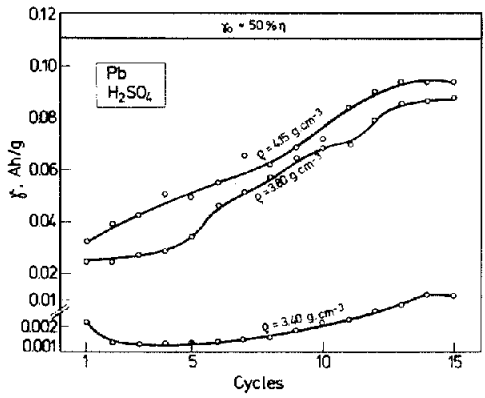

Fig. 1. Increase in specific capacity (γ) of tubular powder electrodes with different PAM densities on cycling.

spines. The value of the capacity, γ_0, calculated at 50%-utilization of the active mass, is also given in this Fig.

It was established that at powder density 3.40 g cm^{-3}, the formation of the active-mass structure proceeds very slowly. When the electrode density is above 3.80 g cm^{-3}, the capacity increases rapidly with cycling. It can be concluded, therefore, that there is a critical density between 3.40 and 3.80 g cm^{-3} above which restoration of the skeleton structure proceeds. In all three electrodes, lead dioxide agglomerates were in mechanical contact with one another.

After completion of the cycling process, the tubular electrodes were cut open. The active mass of the electrodes with density 3.40 g cm^{-3} disintegrated into powder. That of the electrodes with density 3.80 g cm^{-3} preserved the shape of the tube but readily disintegrated on pressure, while the active mass of the electrode with density 4.15 g cm^{-3} retained a cylindrical shape that could only be destroyed under considerable pressure.

Effect of antimony ions in the solution

Electrodes with lead spines were investigated. PbO_2 powder electrodes with density 3.40 and 4.15 g cm^{-3} were used. Three concentrations of antimony ions were studied. Figure 2 shows the changes in capacity during cycling of the electrodes. Antimony ions were added to the solution at the 6th and the 10th cycles. These ions passivate the electrode with PAM density 3.40 g cm^{-3} and stop the formation of the active-mass structure. The higher the concentration of antimony in the solution, the stronger the influence. This effect of antimony is observed only when the active-mass density is close to, or below, the critical value. Figure 2(b) shows that at a density of 4.15 g cm^{-3}, the effect of antimony is negligible.

Figure 3 presents an X-ray pattern of the PbO_2 active mass after cycling a tubular electrode in H_2SO_4 solution. The content of α-PbO_2 is very small; β-PbO_2 is the predominant modification. The lines with interplanar distances $d = 3.12$ Å and $d = 3.50$ Å or 2.80 Å were selected as characteristic diffraction lines for α-PbO_2 and β-PbO_2, respectively.

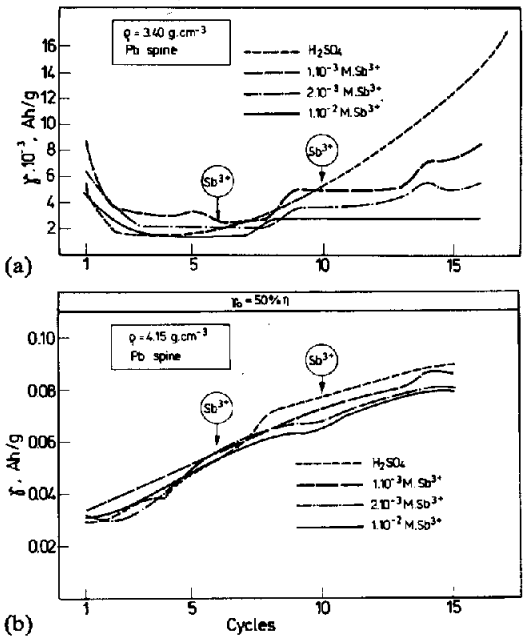

Fig. 2. Effect of antimony ions in H_2SO_4 solution on specific capacity of tubular powder electrodes on cycling.

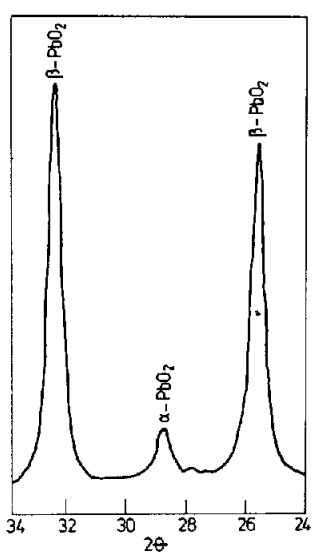

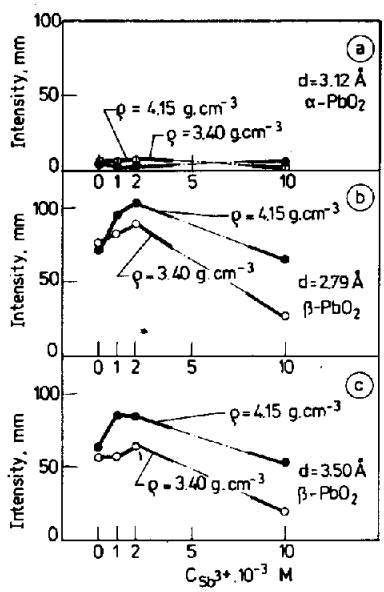

Fig. 3. X-ray diffraction pattern of the positive active mass.

Fig. 4. Dependence of intensity of characteristic diffraction lines for (a) α-PbO_2 ($d = 3.12$ Å), (b) and (c) β-PbO_2 ($d = 3.50$ Å and $d = 2.79$ Å) on concentration of antimony ions in the solution.

Figure 4 shows the changes in intensity of the diffraction lines for α-PbO_2 and β-PbO_2 as a function of the concentration of antimony ions in the solution. The following conclusions can be drawn from the data:

- Antimony ions exert only a slight effect on the intensity of α-PbO_2 diffraction lines
- The intensity of the diffraction lines for β-PbO_2 depends, on the one hand, on the active-mass density and, on the other hand, on the concentration of antimony ions. A higher active-mass density is responsible for a higher degree of crystallinity of β-PbO_2. With increasing the concentration of antimony ions in the solution, the crystallinity of PbO_2 particles increases and passes through a maximum. The consequent decrease in intensity indicates that antimony ions cause amorphization of PbO_2 agglomerates

Effect of antimony in the spine alloy

Tubular powder electrodes were prepared with spines made of lead alloys containing various concentrations of antimony, and powder densities 3.80 and 4.15 g cm^{-3}. Figure 5 presents the dependence of the specific capacity on the antimony content in the alloy after different numbers of cycles.

At a PAM density of 3.80 g cm^{-3}, the electrode capacity during the first cycle is almost independent of the antimony content. At the 5th cycle, the capacity exhibits a two-fold increase when only 0.1% of antimony is present in the alloy. At the 10th and 15th cycles, the difference in capacity of pure lead and lead–antimony electrodes becomes smaller.

At a PAM density of 4.15 g cm^{-3}, the presence of antimony in the spine alloy has a pronounced positive effect, even during the first cycle. At the 10th, and especially at the 15th cycle, even electrodes with Pb–0.15wt.%Sb spines reach 50% utilization of the active mass. Thus, the effect of antimony is more pronounced at an active-mass density of 4.15 g cm^{-3} than at a density of 3.80 g cm^{-3}.

Figure 6 presents TEM micrographs of the active mass of electrodes with lead spines containing 0.1, 2, 6 and 9 wt.% antimony in the alloy. These micrographs show that the active mass is built up of particles of various sizes that are interconnected in microporous agglomerates. The latter exhibit nonhomogeneous electron transparency. As already shown earlier [42, 43], the dense concentrated zones have an α-PbO_2 or β-PbO_2 crystal lattice, while the electron-transparent zones are amorphous, hydrated and gel-like. The contact between the particles is realized through their hydrated surfaces, whereby the gel-like matter passes from one particle to the other, most often divided by clearly visible boundaries of less-concentrated gel mass. The latter may

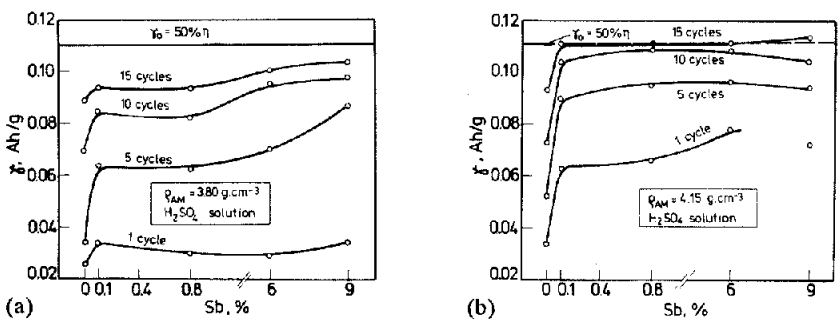

Fig. 5. Effect of antimony content in spine alloy on specific capacity of tubular powder electrodes at 1st, 5th, 10th and 15th cycle: (a) powder density of 3.80 g cm^{-3}; (b) of 4.15 g cm^{-3}.

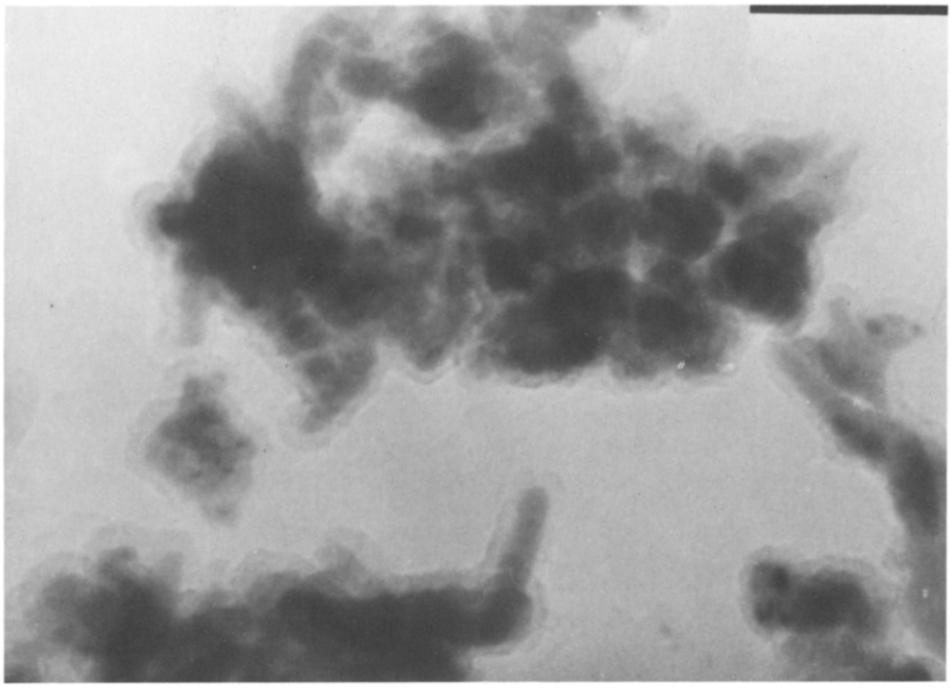

(a)

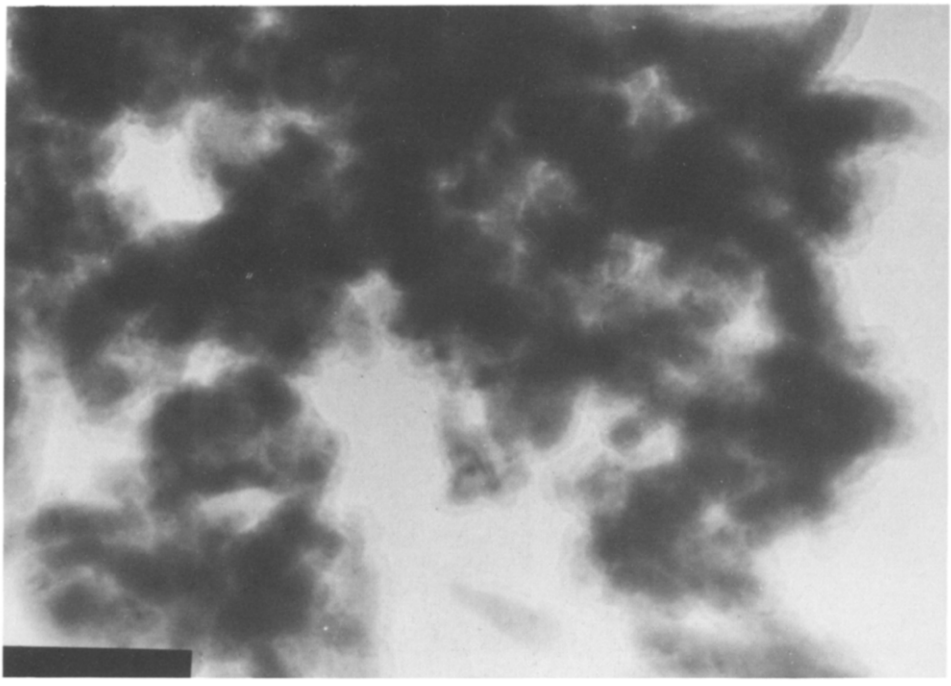

(b)

Fig. 6. *(continued)*

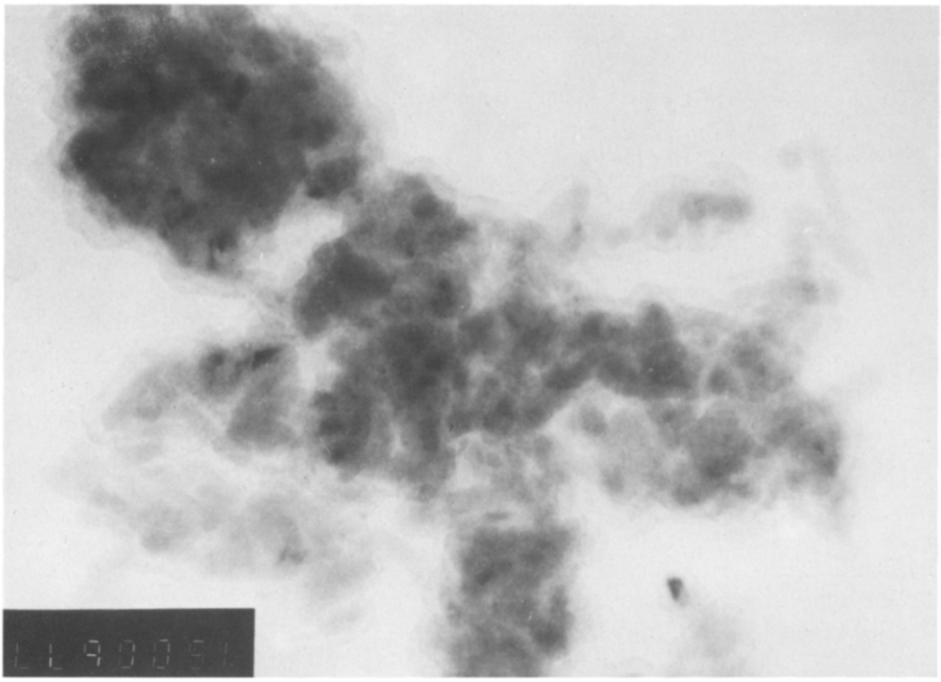

(c)

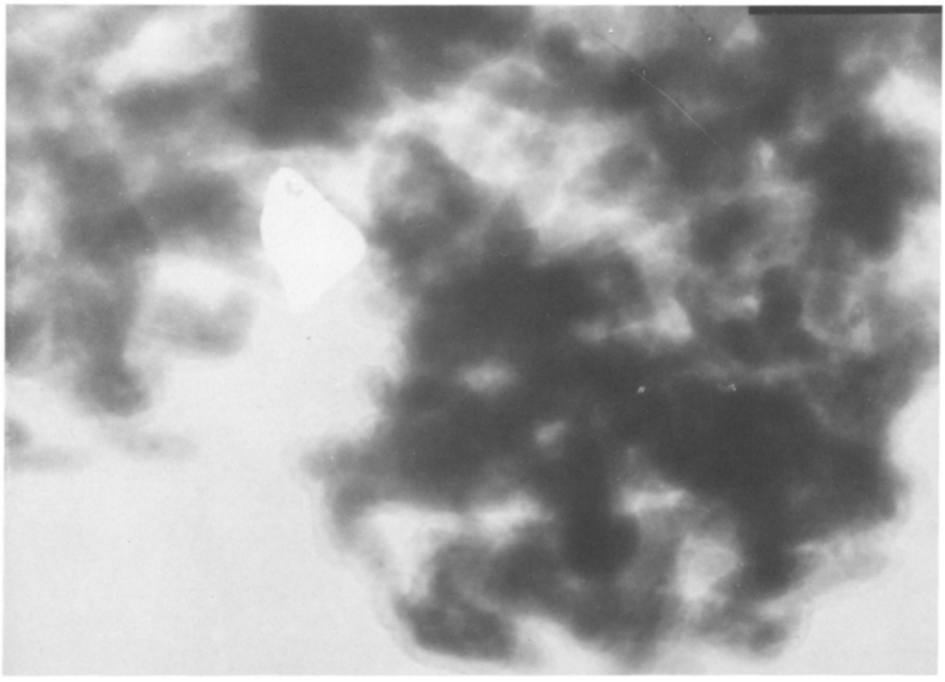

(d)

Fig. 6. (a) Transmission electron microscopy pictures of PAM after cycling of tubular powder electrodes with: (a) Pb–0.1wt.%Sb spines; (b) Pb–2wt.%Sb spines; (c) Pb–6wt.%Sb spines; (d) Pb–9wt.%Sb spines. Magnification $\times 150\,000$.

enclose spaces with strongly diluted gel or empty of mass. These spaces act as micropores in the agglomerates. Crystal zones occupy considerable parts of the particle volume (dark spots in Fig. 6).

TEM micrographs of the agglomerates show that, with increasing the antimony content in the spine alloy, the boundaries between the particles are blurred and they are transformed into a continuous gel-like mass. This undoubtedly increases the amorphization of the agglomerates. The transfer of ions takes place from the solution to the bulk of the agglomerates through the pores/channels with low gel concentration. This process is needed for the discharge reaction to proceed.

Effect of antimony ions in solution and lead–antimony spines

Four alloys were selected with antimony content 0.1, 0.8, 6 and 9 wt.%, respectively. Four powder electrodes were prepared from each alloy with a powder density 3.80 g cm^{-3}, and another four with a density of 4.15 g cm^{-3}. All electrodes were subjected to 5 charge/discharge cycles in H_2SO_4 of 1.28 sp.gr. At the 6th cycle, three electrodes from each type were placed in H_2SO_4 solution (1.28 sp.gr.) with addition of antimony in different concentrations: 10^{-3}, 2×10^{-3} and 10^{-2} M. The fourth electrode from each type was cycled further in the initial acid solution.

Capacity curves for electrodes with Pb–0.1wt.%Sb and Pb–0.8wt.%Sb spines are presented in Fig. 7(a), and those for electrodes with spines containing 6 and 9 wt.% antimony in the alloy are given in Fig. 7(b). The following conclusions can be drawn from the experimental results.

- Electrodes immersed in antimony-containing solutions exhibit slightly lower capacity on cycling than electrodes in pure H_2SO_4
- During initial cycling, electrodes with a powder density of 4.15 g cm^{-3} exhibit almost twice the capacity of those with density 3.80 g cm^{-3}. After the 5th cycle, this difference diminishes and reaches negligible values at the 15th cycle. For a given concentration of antimony ions in the solution, the higher the content of antimony in the alloy the smaller the difference between the capacities of electrodes with the two densities of PAM. At the 15th cycle, this difference is from 0.02 to 0.025 A h g^{-1} for Pb–0.1wt.%Sb electrodes, and only 0.005 A h g^{-1} for Pb–9wt.%Sb electrodes
- Electrodes with a PAM density of 4.15 g cm^{-3} show a sufficiently organized structure between the 8th and the 11th cycles to ensure 50% utilization of the active mass. For electrodes with a density of 3.80 g cm^{-3}, only those with 9 wt.% antimony in the spine alloy reach 50% utilization at the 15th cycle.

Figure 8 presents the intensities of the diffraction lines that correspond to the interplanar distances 3.50 and 2.80 Å for β-PbO_2 in the above electrodes. The following conclusions can be drawn.

- Higher density active masses have higher crystallinity
- An increased content of antimony ions in the solution leads to certain changes in the crystallinity of the active mass. These changes depend on both the type of alloy used and the active mass density
- On comparing Figs. 7 and 8, it becomes evident that when the active mass is completely built up (15th cycle), there is no linear dependence between the crystallinity of the PAM agglomerates and the electrode capacity. Electrodes with 9 wt.% antimony in the spine alloy show significant differences in the intensities of the β-PbO_2 diffraction lines for the two PAM densities, while their capacities are very close or even equal

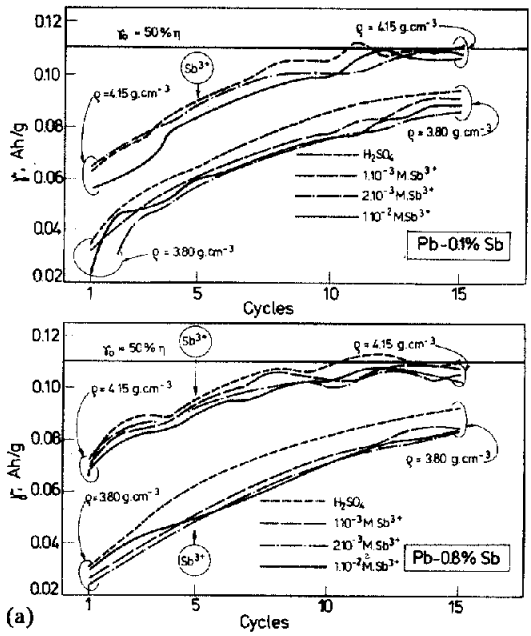

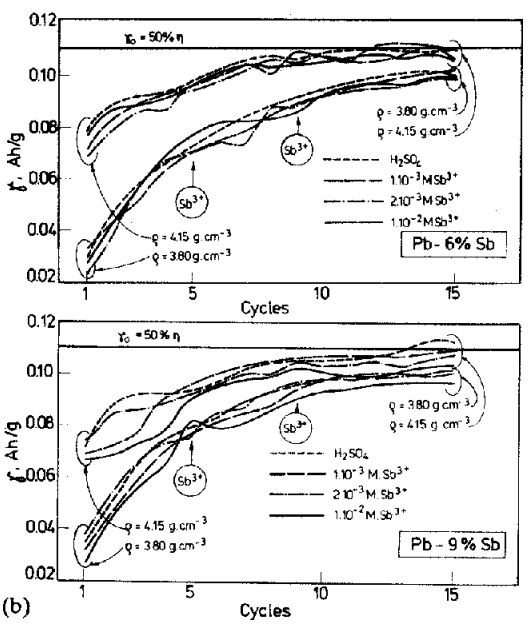

Fig. 7. Capacity changes of tubular powder electrodes on cycling in H_2SO_4 solutions containing different amounts of antimony ions. The spines are made of (a) Pb–0.1wt.%Sb or Pb–0.8wt.%Sb; (b) Pb–6wt.%Sb or Pb–9wt.%Sb.

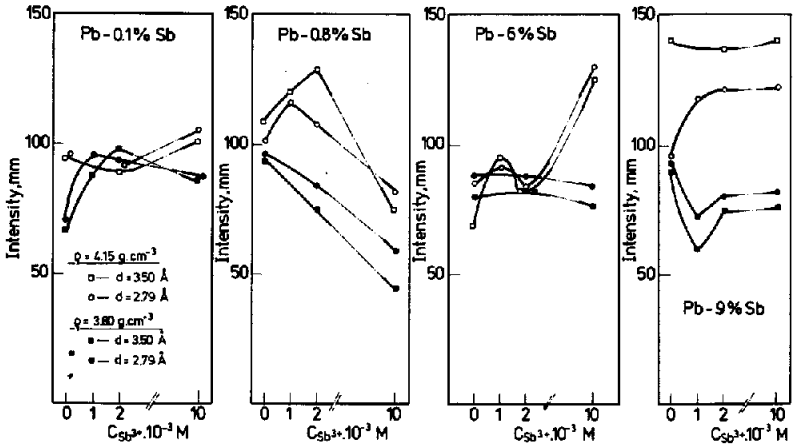

Fig. 8. Changes in intensity of characteristic diffraction lines for β-PbO_2 (d=3.50 Å, d=2.79 Å) in PAM obtained from tubular powder electrodes with lead–antimony spines under action of antimony ions in H_2SO_4 solution.

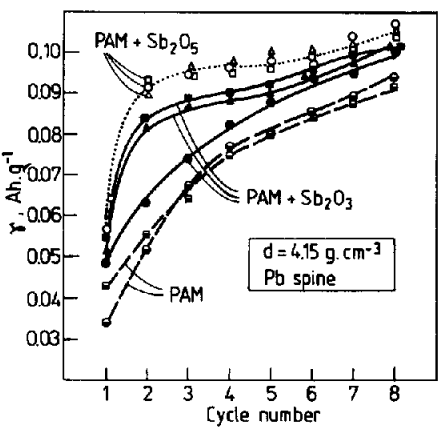

Fig. 9. Changes in specific capacity on cycling of tubular powder electrodes prepared with PAM containing 50 mg of Sb_2O_3 (or Sb_2O_5), or with no additives.

Effect of valency of antimony ions

Electrodes with a density of 4.15 g cm^{-3} were prepared. A 50 mg portion of Sb_2O_3 or Sb_2O_5 was added to the PAM and the latter was thoroughly homogenized. Parallel investigations of three electrodes with each additive and two reference electrodes with no additive were carried out. Pure-lead spines were used. Figure 9 presents the dependence of the specific capacity on the cycle number. During the first few cycles, Sb_2O_3 and Sb_2O_5 cause an abrupt rise in capacity. These oxides have a similar effect to antimony added to the grid alloy. Sb_2O_5 is more beneficial than Sb_2O_3. It follows, therefore, that the valency of antimony also plays a role in the processes of building up the skeleton structure of the PAM.

Figure 10 presents the intensities of the characteristic diffraction lines for α-PbO_2 and β-PbO_2 at the end of cycling for all seven electrodes. An obvious tendency for

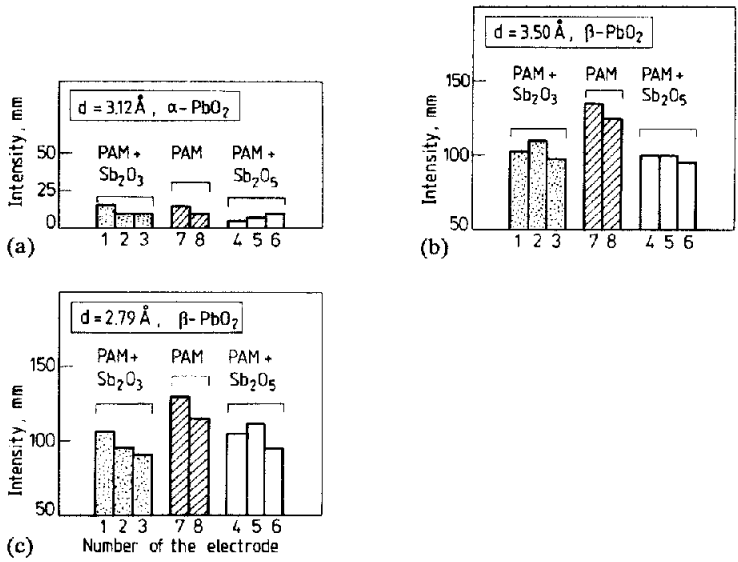

Fig. 10. Intensity of characteristic diffraction lines for α-PbO_2 (d=3.12 Å) or β-PbO_2 (d=3.50 Å and d=2.79 Å) on cycling of tubular powder electrodes with PAM containing 50 mg Sb_2O_3 or Sb_2O_5, or with no additives.

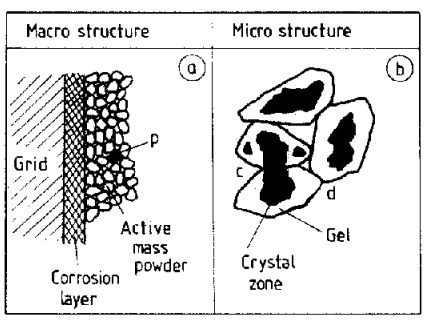

Fig. 11. Models of macrostructure of tubular powder electrodes and of the microstructure of PAM.

the PAM to exhibit amorphization under the action of antimony is observed. No substantial difference is distinguished in the effect of the valency of antimony ions on the PAM crystallinity.

Discussion

A model for the structure and electrical behaviour of PAM

Figure 11(a) shows the macrostructure of the tubular powder electrode. It consists of a spine, a corrosion layer and the PAM particles. Figure 11(b) presents the microstructure of the PAM according to Fig. 6. Particles can come in contact with one another either through their crystal zones (c) or through their gel zones (d) and

thus form agglomerates. Since the surface of PAM particles and agglomerates is hydrated, the powder particles in the tubular electrodes touch one another with their gel zones.

The reduction (discharge) of the PAM on current generation proceeds via two reactions. The first (electrochemical) reaction occurs in the bulk of the particles and agglomerates, probably at the crystal-zone/gel interface [41, 43], i.e.:

$$PbO_2 + 2H^+ + 2e^- \longrightarrow Pb(OH)_2 \quad (1)$$

The second reaction proceeds at the particle (agglomerate)/H_2SO_4 interface and is associated with the formation of $PbSO_4$, i.e.:

$$Pb(OH)_2 + H_2SO_4 \longrightarrow PbSO_4 + 2H_2O \quad (2)$$

For reaction (1) to proceed, hydrogen ions (protons) and electrons have to enter simultaneously the particles (agglomerates). This is a double-injection process or proton-electron mechanism [41–43]. Most probably, the slowest stage of reaction (1) is the transport of electrons and protons to the site of the electrochemical reaction. For reaction (1) to proceed in particle 'p' (Fig. 11(a)), hydrogen ions should pass along the pores of the PAM to particle 'p' and then, through proton conductivity, in the particle itself to the site of the reaction. Electrons have to pass from the plate grid through the corrosion layer, and then through the gel and crystal zones of the agglomerates to particle 'p'.

The electron conductivity of the gel zones will be influenced by the density of the PAM, the ratio between the crystal and gel zones (which is determined by the conditions of PAM preparation and the method of charging), and dopants.

Influence of PAM density on bridge electron conductivity of gel zones

Figure 1 shows that there is a critical active-mass density below which interconnection of the agglomerates of the powder electrode proceeds either extremely slowly or not at all. Using the gel-crystal concept of PAM, this phenomenon can be explained in the following way. For a given agglomerate to take part in the current generation process, the gel zones of this agglomerate should be connected to those of the adjacent ones or of the corrosion layer in such a way as to form uninterrupted polymer chains along which electrons will move for reaction (1) to proceed. If the bridge polymer chains are not formed, this agglomerate will be excluded from the current generation process.

Figures 4 and 8 show that the active mass with density 4.15 g cm^{-3} has higher crystallinity than that with density 3.80 g cm^{-3}. The greater the amount of substance in a unit volume (i.e., the smaller the pore volume), the greater will be the volume of the crystal zones. It is possible, however, that PAM density also exerts an influence on the equilibrium crystal/amorphous zones. With increasing the density of PAM, a certain dehydration of the gel zones proceeds (whereby water is evolved). In this case, the distances between the crystal zones in the particles decrease and hence the bridges between them become shorter. The number of parallel polymer chains that interconnect the crystal zones in PAM particles might be increased, too. Thus, a greater number of particles would be involved in the current generation process. Figures 2 and 7 show that tubular electrodes with higher PAM density have higher capacity. This is an indirect proof of the assumption that the capacity of tubular powder electrodes is determined by the electron conductivity of the gel zones in PAM.

Effect of antimony ions on crystal/gel-zone equilibrium

Dawson *et al.* [44] have studied the type of antimony (III) ions formed at different concentrations of H_2SO_4. At H_2SO_4 concentrations between 0.2 M and 12 M, SbO^+ ions are formed. Below 2 M H_2SO_4, there is evidence of the formation of hydrated species $((H_2O)_2Sb(OH)_2)^+$ and/or $(SbO(OH)_2)^-$. In the region from 2 to 6 M H_2SO_4, $(SbOSO_4)^-$ ions are stable, and at concentrations between 14 and 16 M, antimony is found in the form of $(SbO(SO_4))^-$ ions. Our investigations were conducted in 4.5 M H_2SO_4 solution, which means that the $(SbOSO_4)^-$ type of antimony ions are expected.

As established earlier [45], there is an equilibrium between the crystal and amorphous zones in the particles and agglomerates of the PAM:

$$\underset{\text{crystal zones}}{PbO_2 + H_2O} \rightleftharpoons \underset{\text{amorphous zones}}{PbO(OH)_2} \qquad (3)$$

The amorphous zones, on their part, are in equilibrium with ions in the solution that fills both the micropores and the macropores of the PAM. As agglomerates and particles are an open system, an ion exchange occurs between them and the solution. Anions and cations in the solution are in equilibrium with H^+ and OH^- ions of the hydrated zones [45].

Figure 4 shows that when a tubular powder electrode is immersed in 4.5 M H_2SO_4 solution containing antimony ions, or when the PAM contains Sb_2O_3 or Sb_2O_5 (Fig. 10), the antimony ions enter the hydrated zones of the agglomerates and cause a shift in the equilibrium of eqn. (3) in the direction of amorphization. This is possible if antimony ions penetrate into the surface layers of the crystal zones and, thereby, cause hydration and disintegration, i.e., increase the volume of the gel zones.

Effect of spine antimony on properties of PbO_2 gel-crystal system

Dawson *et al.* [6] have established that antimony(V) species are formed during anodic corrosion of the grid of positive battery plates. These species get into the pore solution in the form of complex ions $(Sb_3O_9)^{3-}$ that are absorbed by the active mass. Then, $(Sb_3O_9)^{3-}$ ions enter the pore solution in the positive plate during the discharge and are reabsorbed during the next charge.

The electrodes were subjected to pretreatment (oxidation for 45 min) to allow the formation of a corrosion layer on the spines. According to the findings of Dawson *et al.* [6], $(Sb_3O_9)^{3-}$ ions would be formed during this period. Figures 5 and 7 show that antimony in the spine alloy increases significantly the capacity of tubular powder electrodes. The difference in capacity, $\Delta\gamma = \gamma_{Pb\text{-}Sb} - \gamma_{Pb}$, for tubular electrodes prepared with lead–antimony and pure-lead spines is presented in Fig. 12 for the two powder densities and the four types of alloy used. This difference has been calculated for the

TABLE 1

Cycle number	$(\gamma_{4.15} - \gamma_{3.80})_{Pb}$ (A h g^{-1})	$(\gamma_{4.15} - \gamma_{3.80})_{Pb\text{-}Sb}$ (A h g^{-1})
1	0.0075	0.0300
5	0.0175	0.0260
10	0.0075	0.0100
15	0.0062	0.0090

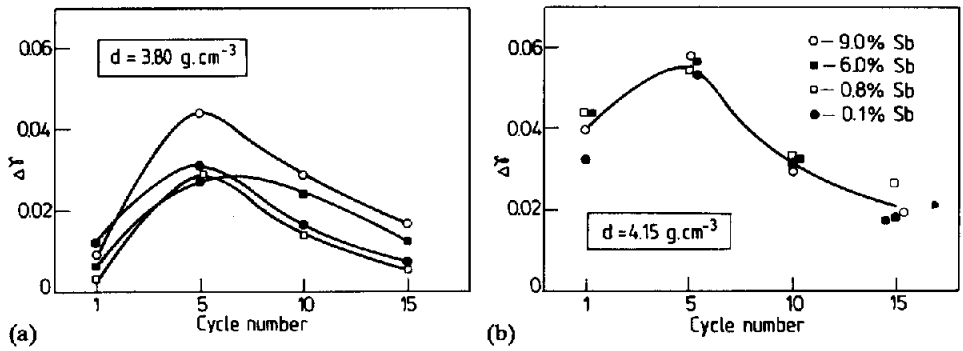

Fig. 12. Difference between the specific capacities of powder electrodes with lead–antimony and pure lead spines at 1st, 5th, 10th and 15th cycle.

1st, 5th, 10th and 15th cycles from the data in Fig. 5. It can be seen that antimony increases the capacity of tubular powder electrodes in the first cycle for both PAM densities. This is due to the $(Sb_3O_9)^{3-}$ ions (according to Dawson *et al.* [6]), increasing the electron conductivity of the gel zones of the agglomerates. Adsorbed either on the lead hydroxide polymer chains or at the interface crystal/amorphous zones, antimony ions reduce the potential barriers that electrons have to overcome on their way along the polymer chain or when hopping from one polymer chain to the other. Such an effect reduces the specific resistance of the gel. This allows a greater number of agglomerates to take part in the current generation process and hence the electrode capacity is high. Thus, $(Sb_3O_9)^{3-}$ ions act as binding elements. With cycling, the amount of oxidized antimony grows and its effect is expanded over a greater number of agglomerates in the powder electrode. It can be seen that the curves in Fig. 12 keep rising from the first to the fifth cycle. They pass through a maximum and start to decline thereafter. This profile of the curves is due to the fact that antimony facilitates the capacity curve of electrodes with Pb–Sb spines to reach faster the state of saturation than electrodes with pure-lead spines.

Figure 12 shows that the increase in capacity is only slightly dependent on the content of antimony in the alloys for an active mass density of 3.80 g cm^{-3}. At 4.15 g cm^{-3}, the capacity increase is almost independent of the antimony content in the spine alloy. This indicates that the curve of the effect of antimony versus the concentration of antimony ions reaches a state of saturation at low antimony concentrations. Antimony exerts a fairly strong influence on the electron conductivity of gel zones. Even Pb–0.1wt.%Sb spines are capable of supplying sufficient antimony ions to cause an increase in conductivity of the gel zones of the agglomerates.

The higher the density of the PAM in the tubular electrode, the greater the capacity difference, i.e., the stronger the effect of antimony. Table 1 presents the effect of PAM density on the capacity for a given cycle. $\Delta\gamma_{Pb} = (\gamma_{4.15} - \gamma_{3.80})_{Pb}$ for electrodes with lead spines at both PAM densities, and $\Delta\gamma_{Pb\text{–}Sb} = (\gamma_{4.15} - \gamma_{3.80})_{Pb\text{–}Sb}$ are the analogous values for electrodes with lead–antimony spines. It can be concluded from the data that the difference $\Delta\gamma_{Pb\text{–}Sb} - \Delta\gamma_{Pb} > 0$. In the above expression, the effect of PAM density on the electrode capacity is eliminated and the influence of antimony on the electron conductivity of gel zones (according to the gel-crystal model) is presented in a plain form.

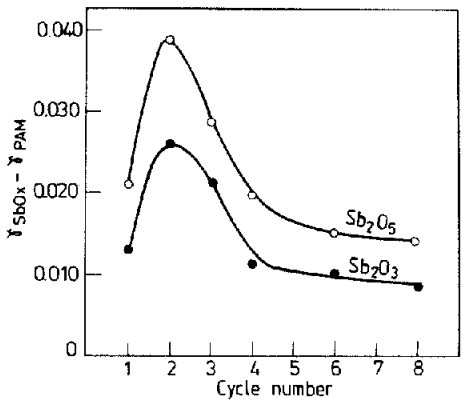

Fig. 13. Difference between the specific capacities of powder electrodes with lead spines containing 50 mg Sb_2O_3 or Sb_2O_5, and of such with no additives, on cycling.

Antimony makes the PAM structure less dependent on the changes in the PAM density. The PAM agglomerates are also in electrical contact with each other at lower PAM densities and this ensures higher positive plate capacity.

Effect of antimony added to PAM or solution

Figure 13 presents the dependence of the difference in capacity of tubular powder electrodes with Sb_2O_3 or Sb_2O_5 (denoted generally as γ_{SbO_x}) and that of the electrodes containing no antimony versus the number of cycles. The data from Fig. 9. were used.

The curves are similar in profile to those presented in Fig. 12(b), i.e., the curve for Sb_2O_5-containing electrodes is ~30% lower than that for antimony added to the alloy (Fig. 12). This may be an indication that similar processes take place in both cases.

For electrodes with addition of Sb_2O_3, the capacity difference ($\gamma_{SbO_x} - \gamma_{H_2SO_4}$) is smaller. It can be assumed that when Sb_2O_3 is dissolved in the pore solution, it is partially oxidized to antimony(V) and acts as such. It is also known that the solution in the pores of the positive active mass has a lower H_2SO_4 concentration; it is neutral and even slightly alkaline in the pores of the agglomerates [43]. It is therefore difficult to say which antimony ion species will be formed from dissolution of the Sb_2O_3. One fact is obvious, however, that lower-valency antimony ions exert a weaker effect on the electron conductivity of gel zones in the agglomerates and on the capacity.

The results presented in Fig. 2 show that $(SbOSO_4)^-$ ions have a slightly inhibiting effect on the electron conductivity of gel zones. As mentioned earlier, the reverse effect is observed with $(Sb_3O_9)^{3-}$ ions (Figs. 5, 7 and 11). When the two types of antimony ions are present in the solution and in PAM (Fig. 7), the influence of the $(SbOSO_4)^-$ ions is suppressed by the action of their $(Sb_3O_9)^{3-}$ counterparts. Consequently, each ion species of a given element displays a specific effect on the electrical properties of the gel-crystal lead dioxide system. The search for appropriate dopants to the PAM may prove an important approach towards improving the capacity performance of lead/acid batteries.

References

1 A. F. Hollenkamp, *J. Power Sources, 36* (1991) 567–585.
2 J. Burbank, *J. Electrochem. Soc., 104* (1957) 693–701.
3 W. Hermann and G. Propstl, *Z. Elektrochem., 61* (1957) 1154–1160.
4 J. Burbank, *J. Electrochem. Soc., 111* (1964) 765–770; *111* (1964) 1112–1118.
5 E. J. Ritchie and J. Burbank, *J. Electrochem. Soc., 117* (1970) 299–305.
6 J. L. Dawson, M. I. Gillibrand and J. Wilkinson, in D. H. Collins (ed.), *Power Sources 3,* Oriel, Newcastle upon Tyne, 1970, pp. 1–9.
7 H. S. Panesar, in D. H. Collins (ed.), *Power Sources 3,* Oriel, Newcastle upon Tyne, 1970, pp. 79–89.
8 J. Burbank, *J. Electrochem. Soc., 118* (1971) 525–532.
9 D. E. Swets, *J. Electrochem. Soc., 120* (1973) 925–926.
10 M. J. Brennan, B. N. Stirrup and N. A. Hampson, *J. Appl. Electrochem., 4* (1974) 49–52.
11 S. Feliu and M. Morcillo, *Corros. Sci., 15* (1975) 593.
12 J. L. Weininger and E. G. Siwek, *J. Electrochem. Soc., 123* (1976) 602–606.
13 T. F. Sharpe, *J. Electrochem. Soc., 124* (1977) 168–174.
14 J. P. Carr, N. A. Hampson and R. Taylor, *J. Electroanal. Chem., 33* (1977) 109–116.
15 A. A. Abdul Azim and A. A. Ismail, *J. Appl. Electrochem., 7* (1977) 119–125.
16 T. G. Chang, M. M. Wright and E. M. L. Valeriote, in D. H. Collins (ed.), *Power Soruces 6,* Academic Press, London, 1977, pp. 69–88.
17 S. Hattori, M. Yamaura, M. Kono, M. Yamane, H. Nakashima and J. Yamashita, *ILZRO Project LE-253 Final Rep.; Project LE-276 (Prog. Rep. No. 1),* International Lead Zinc Organization, Research Triangle Park, NC, 1978.
18 A. Arifuku, H. Yoneyama and H. Tamura, *J. Appl. Electrochem., 9* (1979) 629–634; 635–641.
19 B. K. Mahato, *J. Electrochem. Soc., 126* (1979) 365–374.
20 F. Caldara, A. Delmastro, G. Fracchia and M. Maja, *J. Electrochem. Soc., 127* (1980) 1869–1876.
21 I. K. Gibson, K. Peters and F. Wilson, in J. Thomson (ed.), *Power Sources 8,* Academic Press, London, 1980, pp. 565–571.
22 N. A. Hampson, S. Kelly and K. Peters, *J. Appl. Electrochem., 10* (1980) 91–96; 261–267.
23 A. Arifuku, H. Yoneyama and H. Tamura, *J. Appl. Electrochem., 10* (1980) 749–755.
24 D. Bayrett, M. T. Frost, J. A. Hamilton, K. Harris, I. R. Harrowfield, J. F. Moresby and D. A. J. Rand, *J. Electroanal. Chem., 118* (1981) 131–137.
25 N. M. Cong, A. Ejjenne, J. Brenet and P. Faber, *J. Appl. Electrochem., 11* (1981) 373–379.
26 A. Arifuku, H. Yoneyama and H. Tamura, *J. Appl. Electrochem., 11* (1981) 357–363.
27 K. Fuchida, K. Okada, S. Hattory, M. Kono, M. Yamane, T. Takayama, J. Yamashita and Y. Nakayama, *ILZRO Project LE 276 Final Rep., (Prog. Rep. No. 8),* International Lead Zinc Organization, Research Triangle Park, NC, 1982.
28 A. Boggio, M. Maja and N. Penazzi, *J. Power Sources, 9* (1983) 221–230.
29 T. Rogachev, G. Papazov and D. Pavlov, *J. Power Sources, 10* (1983) 291–297.
30 T. G. Chang, in K. R. Bullock and D. Pavlov (eds.), *Proc. Symp. Advances in Lead/Acid Batteries,* Proc. Vol. 84-14, The Electrochemical Society, Pennington, NJ, 1984, pp. 86–97.
31 S. Webster, P. J. Mitchell and N. A. Hampson, *J. Electrochem. Soc., 133* (1986) 133–136; 137–139.
32 D. Pavlov and B. Monahov, *J. Electroanal. Chem., 218* (1987) 135–141.
33 M. N. C. Ijomah, *J. Electrochem. Soc., 134* (1987) 2960–2966.
34 R. J. Hill, *J. Solid State Chem., 71* (1987) 12–17.
35 D. Pavlov, A. Dakhouche and T. Rogachev, *J. Power Sources, 30* (1990) 117–129.
36 D. Pavlov, *J. Power Sources, 33* (1991) 221–229.
37 T. Laitinen, K. Salmi, G. Sundholm, B. Monahov and D. Pavlov, *Electrochim. Acta, 36* (1991) 605–613.
38 D. Pavlov, B. Monahov, G. Sundholm and T. Laitinen, *J. Electroanal. Chem., 305* (1991) 57–72.
39 E. M. L. Valeriote, A. Heim and M. S. Ho, *J. Power Sources, 33* (1991) 187–212.
40 J. Garche, E. Voss, R. F. Nelson and D. A. J. Rand, *J. Power Sources, 36* (1991) 405–413.

41 D. Pavlov, *J. Electrochem. Soc., 139* (1992) 3075–3080.
42 D. Pavlov, I. Balkanov, T. Halachev and P. Rachev, *J. Electrochem. Soc., 136* (1989) 3189–3197.
43 D. Pavlov, I. Balkanov and P. Rachev, *J. Electrochem. Soc., 134* (1987) 2390–2398.
44 J. L. Dawson, J. Wilkinson and M. I. Gillibrand, *J. Inorg. Nucl. Chem., 32* (1970)501–517.
45 D. Pavlov and I. Balkanov, *J. Electrochem. Soc., 139* (1992) 1830–1835.